Journal of Molecular Catalysis A: Chemical 348 (2011) 42–54

Contents lists available at ScienceDirect

Journal of Molecular Catalysis A: Chemical

journal homepage: www.elsevier.com/locate/molcata

Ag promoted $La_{0.8}Ba_{0.2}MnO_3$ type perovskite catalyst for N_2O decomposition in the presence of O_2, NO and H_2O

Suresh Kumar[a], Y. Teraoka[b], Amish G. Joshi[c], S. Rayalu[a], Nitin Labhsetwar[a,*]

[a] National Environmental Engineering Research Institute (NEERI-CSIR), Nehru Marg, Nagpur 440020 India
[b] Department of Energy and Material Sciences, Faculty of Engineering Sciences, Kyushu University, Kasuga, Fukuoka 816-8580, Japan
[c] National Physical Laboratory, Dr. K.S. Krishnan Road, New Delhi 110 012, India

ARTICLE INFO

Article history:
Received 9 May 2011
Received in revised form 26 July 2011
Accepted 27 July 2011
Available online 5 August 2011

Keywords:
N_2O decomposition
Perovskite
Silver promoted perovskite
Lanthanum manganate
Support

ABSTRACT

$La_{0.8}Ba_{0.2}MnO_3$ and silver promoted $La_{0.8}Ba_{0.2}MnO_3$ type perovskite catalysts have been studied for N_2O decomposition reaction. These catalysts were prepared by co-precipitation process followed by impregnation method for Ag incorporation. These catalysts were characterized in detail by means of ICP-OES, XRD, BET, SEM, STEM, EDX, XPS, O_2-TPD and H_2-TPR analysis. An appreciable increase in catalytic activity was achieved by promoting the lanthanum manganate by Ba as well as Ag. The promotional effect of Ag was observed maximum at 1 wt% optimized loading. The effect of O_2, NO and H_2O on the bare and Ag promoted catalysts for N_2O decomposition was also investigated. The catalytic activity for N_2O decomposition was significantly increased by Ba substitution as well as by Ag promotion. The activity of these improved catalysts was also relatively less affected in presence of oxygen, water vapour and NO, thereby showing promotional effect of silver on N_2O decomposition. These catalysts were also prepared in supported forms using ceramic honeycomb via in situ co-precipitation method, and then tested for N_2O decomposition reaction. Supported catalysts show equally good catalytic activity towards N_2O decomposition. XPS and O_2-TPD studies suggest that Ag incorporation results in increase of Mn^{4+}/Mn^{3+} ratio of $La_{0.8}Ba_{0.2}MnO_3$ catalyst. TPR studies also provided the clear evidence to this effect. This improved redox property of Ag promoted perovskite catalyst was correlated to its enhanced catalytic activity for N_2O decomposition.

1. Introduction

Nitrous oxide has been identified as a potential contributor to the destruction of ozone in the stratosphere as well as a relatively strong green house gas [1–5]. It has been recognized that the migration of nitrous oxide (N_2O) into the stratosphere contributes with CFC to ozone layer depletion [6]. N_2O is also an absorber of Infrared radiation and thus contributes to the green house effect [6,7]. The GWP (global warming potential) of nitrous oxide is 310 times larger than that of CO_2 [8,9]. The estimated amount of N_2O released in the atmosphere is 4.7–7 million ton per year, which is due to both anthropogenic and natural sources [10]. The ambient level of nitrous oxide is 314 ppb, which is constantly increasing in the recent past. The major anthropogenic sources are nitric and adipic acid plants [3,9,11–13]. Nitric acid is increasingly used for fertilizer production and it is manufactured through oxidation of ammonia. During this catalytic oxidation process, nitrous oxide is produced as a byproduct. Approximately 21.7 Tg CO_2 Eq of N_2O was emitted from nitric acid industry in 2007. Emissions increased by 19 percent between 2006 and 2007, which resulted from an increase in nitric acid production driven by increased synthetic fertilizer demand by agriculture sector [9]. Nylon production is also responsible for nitrous oxide emission, in which adipic acid is used as one of the major precursors. Nitrous oxide emitted from adipic acid production during the oxidation of a ketone–alcohol mixture with nitric acid. N_2O emissions from adipic acid industry were estimated to be 5.9 Tg CO_2 Eq in 2007 [9].

Large number of catalysts have been studied for decomposition of N_2O, including noble metals [14–17], metal oxides [18–22] and metal or ion exchanged zeolites [23–25]. At low temperature, noble metal based catalysts show very good activity towards N_2O decomposition. However, these noble metal supported systems are expensive and unstable at high temperature as well as in presence of oxygen [15]. Most of the zeolite based materials are also potential catalysts for decomposition of N_2O at low temperature. Though, some of these materials are significantly affected because of their instability in presence of water vapor [26], development of hydrothermally stable catalysts has significantly improved the prospects. Usually for industrial applications, catalysts with better

* Corresponding author. Tel.: +91 712 2247828, fax: +91 712 2247828.
E-mail address: nk_labhsetwar@neeri.res.in (N. Labhsetwar).

1381-1169/$ – see front matter © 2011 Elsevier B.V. All rights reserved.
doi:10.1016/j.molcata.2011.07.017

chemical and thermal stability as well as lower cost are preferred. Perovskites are promising catalysts with respect to their low cost and thermal stability. Perovskites are usually prepared by following high temperature calcination, which often results in sintered phases with low surface area. The general chemical formula of perovskite is ABO_3, in which A ions can be rare earth, alkaline earth and other large ions, while B ions are generally first row transition metal ions. In this ABO_3 structure, often the coordination number of A cation is 12, while the coordination number of B cation is 6 [27–29]. Their catalytic activity depends on B site cation, however, the "A" site cation can also influence the overall catalytic activity of a catalyst, primarily by effecting the oxidation states of B site cation and thereby changing the overall redox properties of perovskite phase.

Russo et al. studied the $LaCoO_3$ perovskite type catalytic material prepared by solution combustion synthesis for N_2O decomposition and reported that 50% of N_2O conversion was achieved at 455 °C and 490 °C in the absence and presence of 5% of oxygen, respectively [30]. Alini et al. studied several alkaline based perovskite materials such as Ca and Ba towards decomposition of N_2O. They reported that $CaMn_{0.7}Cu_{0.3}O_3$ catalyst had highest activity of 95% conversion at 550 °C as well as stable catalytic activity for a period of 1400 h stream, which contains stimulated industrial gas coming from an adipic acid plant [31]. Buciuman studied the alkali as well as alkaline metal substituted $LaMnO_3$ type perovskites for NOx reduction using propene [32]. Liu studied the promotional effect of Ag on the performance of $Ag/La_{0.6}Ce_{0.4}CoO_3$ for the decomposition of NOx [33]. Zhu reviewed the structural and physicochemical properties, as well as electrochemical properties of substituted/promoted perovskites with respect to NOx control [34]. Dacquin et al. studied the catalytic N_2O decomposition on 1 wt% $Pd/LaCoO_3$ and reported the reaction rate of 0.0023 mmol min^{-1} g^{-1} at 460 °C [35].

Extensive research works have been reported on perovskite based catalysts by partially substituting 'A' and 'B' site of the ABO_3 structure. However, reports on substituted/promoted perovskites towards decomposition of N_2O are relatively less. The aim of present research is to develop the catalytic systems based on substituted/promoted perovskite type oxides because of their high thermal stability, low cost and high intrinsic catalytic activity. As perovskites are not easy to support on commercial honeycomb, efforts have been made to study the catalytic activity of present catalysts in supported form as well. This paper describes the synthesis, characterization and catalytic activity of $La_{0.8}Ba_{0.2}MnO_3$, various Ag promoted $La_{0.8}Ba_{0.2}MnO_3$ perovskites and ceramic honeycomb supported perovskites towards N_2O decomposition reaction in the presence and absence of oxygen, water vapour and NO. It was possible to study the effect of Ag promotion on oxidation states of Mn and also on redox properties of perovskite phase. The TPR studies have been carried out to investigate the redox properties of Ba and Ag promoted catalyst. These results along with XPS findings could explain the N_2O decomposition activity of present catalysts, as well as the promotional effect of Ba and Ag.

2. Experimental

2.1. Materials

Laboratory grade lanthanum nitrate (Merck-India Ltd), barium nitrate (Merck-India Ltd), manganese nitrate (Merck-India Ltd), silver nitrate (Merck-India Ltd), liq. ammonia (Merck-India Ltd) were used directly without any further purification. Commercial cordierite honeycomb supports with 400 cpsi and wall thickness of 0.15 mm were used to prepare supported catalysts. Coefficient of thermal expansion of support is 8×10^{-7} to 12×10^{-7} °C^{-1}, with a pore size of 4–15 μm.

2.2. Catalyst synthesis

$La_{0.8}Ba_{0.2}MnO_3$ catalyst was prepared by co-precipitation method except that the Ba was incorporated by impregnation in the co-precipitated mass before the heating step. In this method, 1 M ammonium hydroxide precipitant was added to the aqueous solution of lanthanum nitrate (0.033 mol) and manganese nitrate (0.0413 mol) with stirring (100 rpm) at ambient temperature. After the aging process, the precipitate was filtered and washed with double distilled water until the pH of the filtrate was neutral. The precipitate cake was then soaked with the aqueous solution of barium nitrate (0.0083 mol) and dried at 80 °C for 3 h in a hot plate, followed by calcination at 400 °C for 5 h. The solid mass thus obtained was homogenized by grinding and it was further calcined at 850 °C for 8 h in a muffle furnace.

Ag promoted $La_{0.8}Ba_{0.2}MnO_3$ catalysts were prepared by impregnating Ag into $La_{0.8}Ba_{0.2}MnO_3$ phase after its formation. The $La_{0.8}Ba_{0.2}MnO_3$ powder was soaked with aqueous $AgNO_3$ (0.05, 0.5, 1 and 3 wt%) solution and dried at 80 °C with homogenization. The samples thus obtained were calcined at 450 °C for 5 h to get the Ag properly incorporated on perovskite catalyst.

2.3. Synthesis of supported catalysts

The honeycomb supports used has 400 cpsi cell density with the wall thickness of approximately 0.15 mm. The initial porosity of these supports was in the range of 35–40% with an open frontal area of 65–78%. The supported $La_{0.8}Ba_{0.2}MnO_3$ was prepared by following two steps: (i) preliminary coating of lanthana by in situ precipitation method (approx. 3 wt% referred to the monolith wt.). In this precoating process, the support was soaked in the precipitate slurry that was obtained from lanthanum nitrate and dried by using a hot air blower. This process was repeated for several times to obtain the desired loading of lanthana. Then the coated supports thus obtained were calcined at 500 °C for 4 h, (ii) the catalyst coating (approximately 3 wt% referred to the monolith weight) on these pre-coated support was processed by in situ co-precipitation method, using similar procedure that was used for precoating of lanthana. Finally, the support was calcined at 850 °C for 8 h to obtain the cordierite honeycomb supported perovskite phase.

Honeycomb supported Ag-$La_{0.8}Ba_{0.2}MnO_3$ catalysts were prepared by impregnating Ag into $La_{0.8}Ba_{0.2}MnO_3$ phase after its formation. The supported $La_{0.8}Ba_{0.2}MnO_3$ was soaked with aqueous $AgNO_3$ solution and dried by using hot air blower. This process was repeated a few times to obtain the desired loading. The samples thus obtained were calcined at 450 °C for 5 h as already described.

2.4. Characterization of catalytic materials

Inductively coupled plasma-optical emission spectrometer (ICP-OES) was used to quantify the chemical composition of perovskites as well as Ag content. The ICP-OES analysis has been carried out using Perkin Elmer-Optima 4100 DV instrument. Supported and unsupported catalysts were characterized by X-ray diffraction (XRD) and Brunauer–Emmett–Teller (BET) adsorption methods for the confirmation of perovskite phase formation and determination of specific surface area respectively. The X-Ray diffraction patterns have been recorded using X-ray diffractometer (Rigaku: Miniflex-II-DD34863) operated at 30 kV and 15 mA with a monochromator and using Cu-K_α radiation (k = 0.15418 nm). The additionally generated K_β radiation was filtered by monochromator. The sample was scanned for 2θ range from 15 to 90°. Indexing of XRD peaks was done, by using the ICCD (JCPDS) cards for the respective phases. BET surface area of samples was determined following the standard nitrogen adsorption method using Micromeritics ASAP-2000 instrument. The SEM investigations

were carried out by JEOL JSM-6380A instrument using 10.0 kV acceleration voltages to study the morphology of catalysts. Chemical compositions of the catalysts were determined by ICP-AAS technique after acid digestion. Scanning Transmission Electron Microscopy (STEM) analysis was performed by TECNAI-F20 instrument using 200 kV acceleration voltages to study the surface morphology of the catalysts. EDX analysis was also performed using JED-2300. The sample was coated with platinum. The aim of this analysis was to get information about the presence and distribution of elements on the external surface of the samples.

X-ray Photoelectron Spectroscopy (XPS) measurement were carried out for the $La_{0.8}Ba_{0.2}MnO_3$ and 1 wt% Ag-$La_{0.8}Ba_{0.2}MnO_3$ samples, using a Perkin Elmer 1257 model XPS system, operating at a pressure of 1.9×10^{-8} torr and 1.8×10^{-8} torr, respectively at room temperature with a non-monochromatized Al Kα line at 1486.6 eV, and a hemispherical sector analyzer capable of 0.25 eV resolution. The overall instrumental resolution was about 0.3 eV. Pass energy for survey scan and core level spectra kept at 143.05 and 71.55 eV, respectively.

Temperature-programmed desorption (TPD) and temperature-programmed reduction analysis were performed in a Thermo Quest TPD/R/O 1100 analyzer, equipped with a TCD detector. A fixed bed of catalyst was placed in a quartz tube; prior to each temperature-programmed oxygen desorption (TPD) run, the catalyst was heated up to 800 °C under the helium flow (30 ml/min). After 30 min of isothermal heating at this temperature, the sample was cooled to 25 °C in air flow. Afterwards, helium was fed to the reactor at 10-mL/min-flow rate and kept flowing for 1 h at room temperature in order to purge out any excess oxygen. The catalyst was then heated up to 850 °C at the constant heating rate of 10 °C/min under the same helium flow and, O_2 desorbed during the heating was estimated. For H_2-TPR experiments, the catalyst was pretreated under a flow of argon (25 ml/min) at 300 °C for 30 min and cooled to room temperature under the same flow. The reduction of catalyst was followed by heating the catalyst up to 800 °C at constant heating rate of 10 °C/min under the H_2-Ar flow, and consumption of H_2 during the heating was determined by using a TCD.

2.5. Catalytic activity evaluations

The catalytic decomposition of N_2O was carried out in a fixed-bed, steady state type gas reactor as depicted in Fig. 1. Catalyst sample (0.5 g) was placed in a quartz reactor for catalytic run and temperature of the reactor was maintained by using PID controlled furnace. Prior to the catalytic activity test, the catalysts were pretreated at 400 °C for 2 h in a flow of helium for surface cleaning. The total flow rate (63 SCCM) of high purity 5000 ppm N_2O, and balance He gases were measured by mass flow controllers (Alborg, USA). The effect of co-presence of 5 vol% O_2 and 0.02 vol%. NO was also studied in separate evaluation experiments. The NO content was also followed during the course of N_2O decomposition reaction, to study the effect of catalysts on simultaneous NO oxidation/decomposition. The space velocity used for each run was approximately 7500 h^{-1}. After the catalyst had attained steady state over a period of 30 min at each temperature, the effluent gas was analysed by a gas-chromatograph (Perkin Elmer-Clarus 500) using a Molecular Sieve 5A column (for the analysis of O_2, N_2) and a Porapak column for N_2O as well as by a chemiluminescence based NOx analyzer (Environnement SA) for other products. The similar procedure was used for the evaluation of supported catalysts towards N_2O decomposition. In case of supported catalysts, the space velocity was maintained at approximately 2000 and 50,000 h^{-1} with reference to total volume of catalyst coated honeycomb and catalyst volume, respectively.

The catalytic activity was expressed in terms of conversion (X) of N_2O gas according to the following equation:

$$X_{N_2O} = \frac{P_{N_2O\,in} - P_{N_2O\,out}}{P_{N_2O\,in}}$$

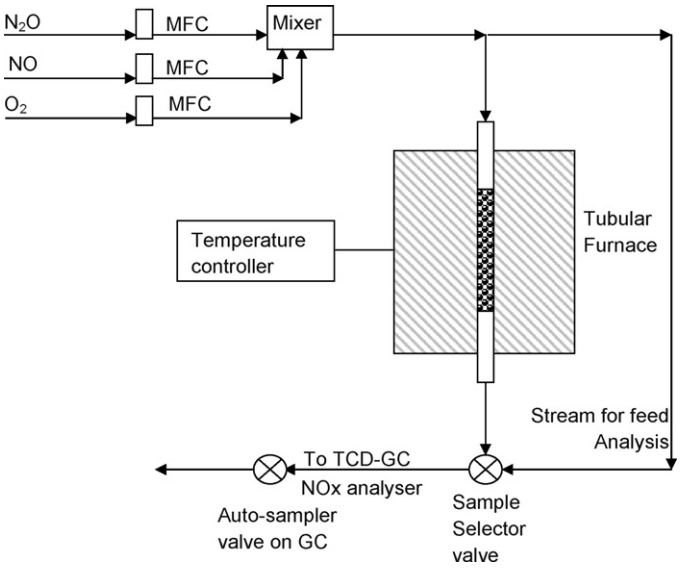

Fig. 1. Schematic diagram of the steady state catalyst evaluation system.

3. Results and discussion

3.1. Catalyst characterization

The chemical composition results obtained by ICP-OES for various Ag loaded $La_{0.8}Ba_{0.2}MnO_3$ catalyst are shown in Table 1. The ICP analysis confirms the presence of targeted chemical compositions as well as amount of Ag in all the samples, which was expected considering the Ag incorporation procedure used. The X-ray diffraction patterns were compared with standard JCPDS cards, which confirm the formation of crystalline $La_{0.8}Ba_{0.2}MnO_3$ phase with perovskite structure (JCPDS 75-0440). Very small amount of La_2O_3 (JCPDS 89-4016) was observed in $LaMnO_3$. The XRD pattern of $La_{0.8}Ba_{0.2}MnO_3$ catalyst shows a very low intensity diffraction peak for Ba_2MnO_3 (JCPDS 75-0193), however, other peaks for this phase were not observed, thereby not confirming the presence of any significant impurity of this phase. The XRD patterns for $La_{0.8}Ba_{0.2}MnO_3$ and various Ag doped $La_{0.8}Ba_{0.2}MnO_3$ perovskite catalysts used in this study are shown in Fig. 2. It was not possible to identify the presence of Ag in catalysts, except when the Ag content was 3 wt%, which indicates the possibility of Ag incorporation in perovskite, leading to its high dispersion. XRD pattern for 3 wt% Ag-$La_{0.8}Ba_{0.2}MnO_3$ shows a weak peak for Ag_2O phase, which is in good agreement with standard data (JCPDS 72-2108). This suggests that a separate Ag_2O phase emerges at higher amount of silver incorporation. This is obvious considering the certain limit of 'A' site substitution in perovskites, which depends on perovskite composition as well as method of preparation. The XRD patterns

Table 1
Quantitative results (%) of Ag on $La_{0.8}Ba_{0.2}MnO_3$ obtained by ICP-OES analysis.

Ag loading on $La_{0.8}Ba_{0.2}MnO_3$ catalyst (wt%)	% of Ag obtained by ICP-OES
0.05	0.045
0.5	0.479
1	0.983
3	3.14

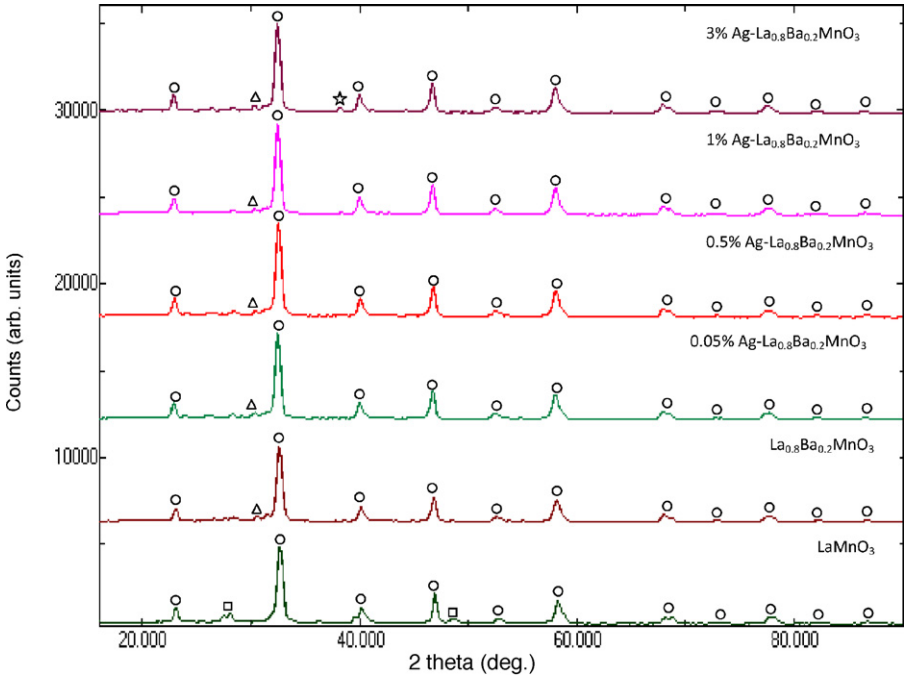

Fig. 2. XRD patterns for $LaMnO_3$, $La_{0.8}Ba_{0.2}MnO_3$ and various $Ag/La_{0.8}Ba_{0.2}MnO_3$: (◯) perovskite; (□) La_2O_3; (△) Ba_2MnO_3;(☆) Ag_2O.

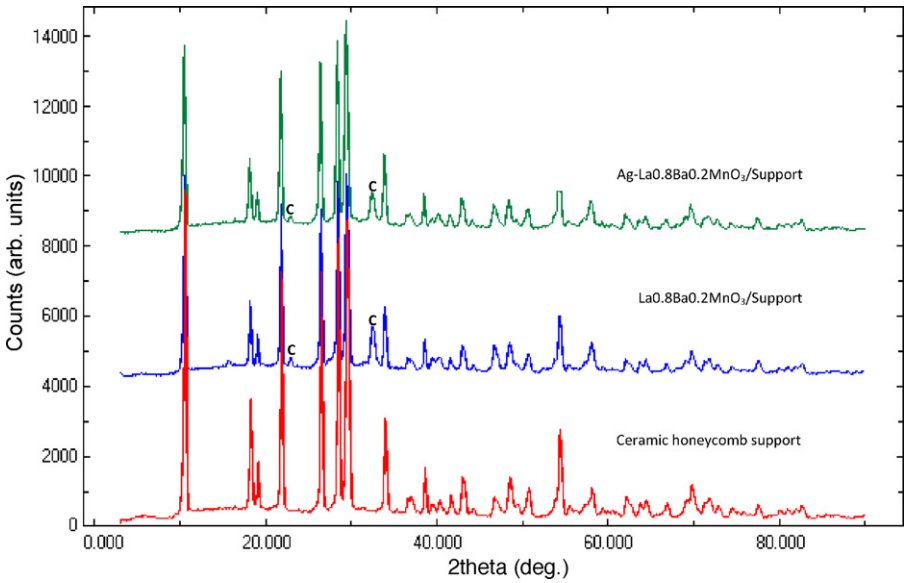

Fig. 3. XRD patterns for ceramic honeycomb supported $La_{0.8}Ba_{0.2}MnO_3$ and $Ag/La_{0.8}Ba_{0.2}MnO_3$ (C: catalyst phase).

of bare ceramic honeycomb support and supported catalysts are compared in Fig. 3. These clearly indicate the formation of perovskite phase on supports as well as its crystalline nature. The present method using co-precipitated mass for the synthesis of perovskite on cordierite honeycomb appears suitable, as perovskite precursors are often reported to be reactive towards cordierite. As we observed in our previous works [36], the precoat of lanthana is also useful to prevent perovskite precursors from reacting with cordierite. In this way, it was possible to support perovskite catalyst on commercially available cordierite support. The BET surface area results are shown in Table 2. The surface area of catalytic materials even after calcination at higher temperature is in the range of about 6–7 $m^2\,g^{-1}$, which is reasonably high considering the highly sintered perovskite phase. BET of supported catalytic materials shows surface area of approximately 4–5 $m^2\,g^{-1}$.

The SEM micrographs in Fig. 4(1 and 2) show that the perovskite powders obtained by co-precipitation method contain agglomerates of perovskite particles. The SEM images of bare ceramic honeycomb support, supported $La_{0.8}Ba_{0.2}MnO_3$ and supported $Ag\text{-}La_{0.8}Ba_{0.2}MnO_3$ are shown in Fig. 5(1–6). The top view image at

Table 2
BET surface area results for various catalysts and support.

Sr. no.	Sample	Surface area ($m^2\,g^{-1}$)
1	$La_{0.8}Ba_{0.2}MnO_3$	7
2	$Ag/La_{0.8}Ba_{0.2}MnO_3$	6
3	Cordierite support	1.2
4	Supported $La_{0.8}Ba_{0.2}MnO_3$	5
5	Supported $Ag/La_{0.8}Ba_{0.2}MnO_3$	4

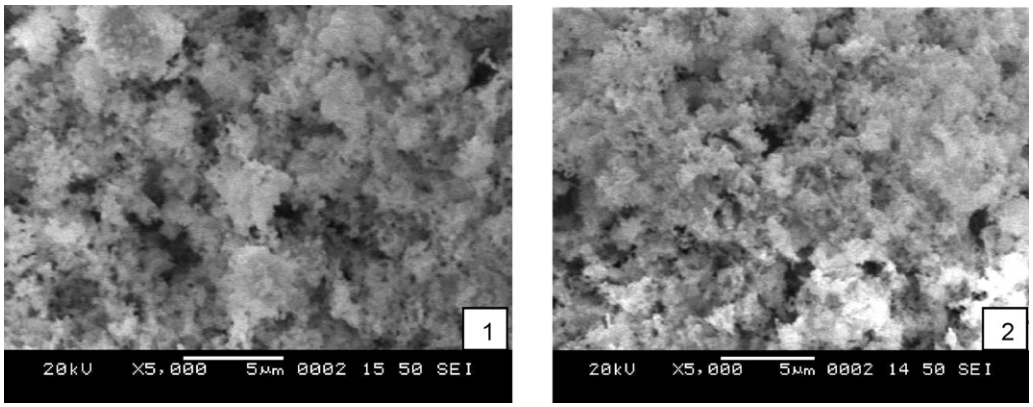

Fig. 4. (1) SEM photograph of $La_{0.8}Ba_{0.2}MnO_3$ (2) SEM photograph of $Ag/La_{0.8}Ba_{0.2}MnO_3$.

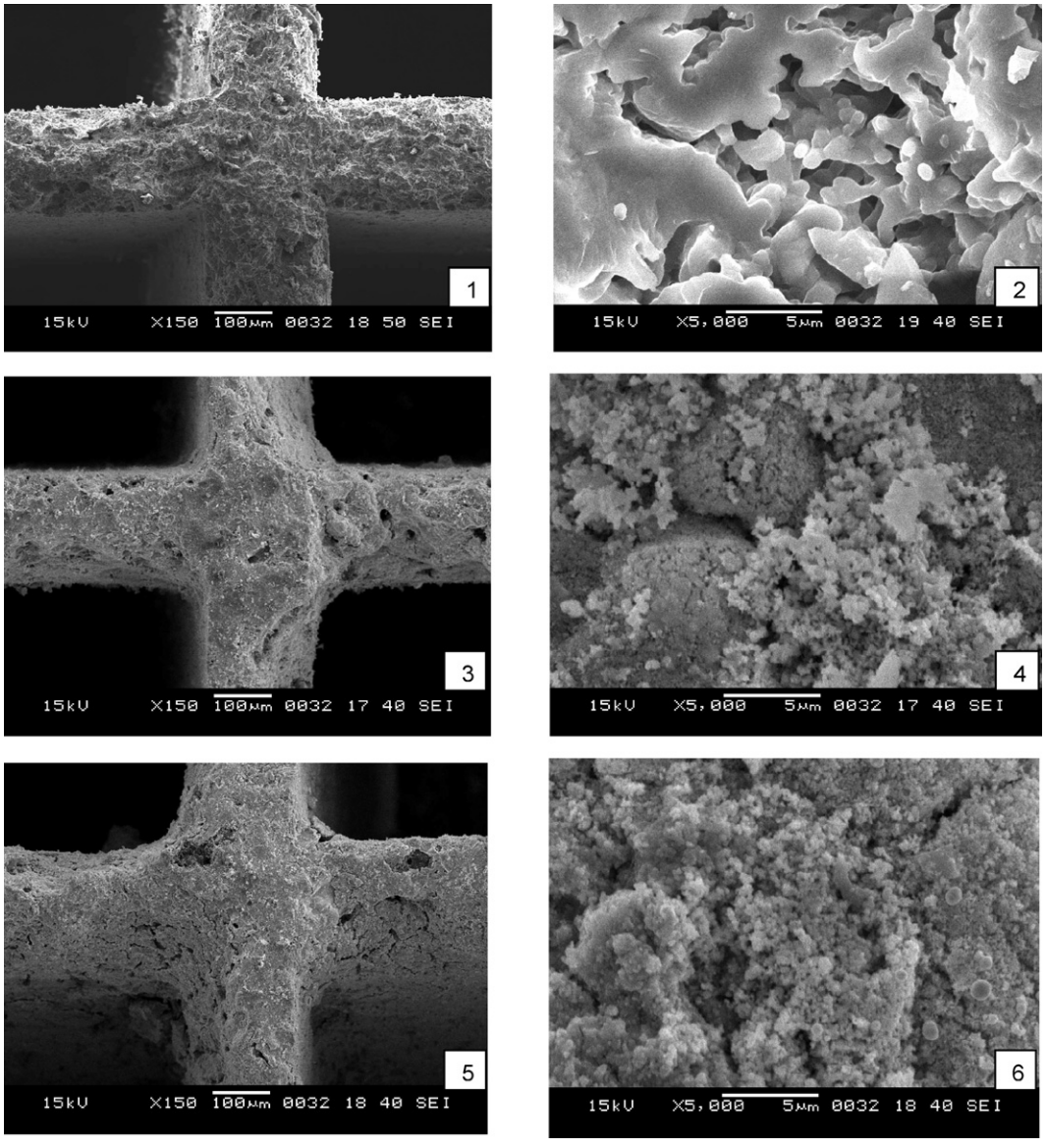

Fig. 5. (1 and 2) SEM photograph of ceramic honeycomb support (top-view). (3 and 4) SEM photograph of supported $La_{0.8}Ba_{0.2}MnO_3$ (top-view). (5 and 6) SEM photograph of supported $Ag/La_{0.8}Ba_{0.2}MnO_3$ (top-view).

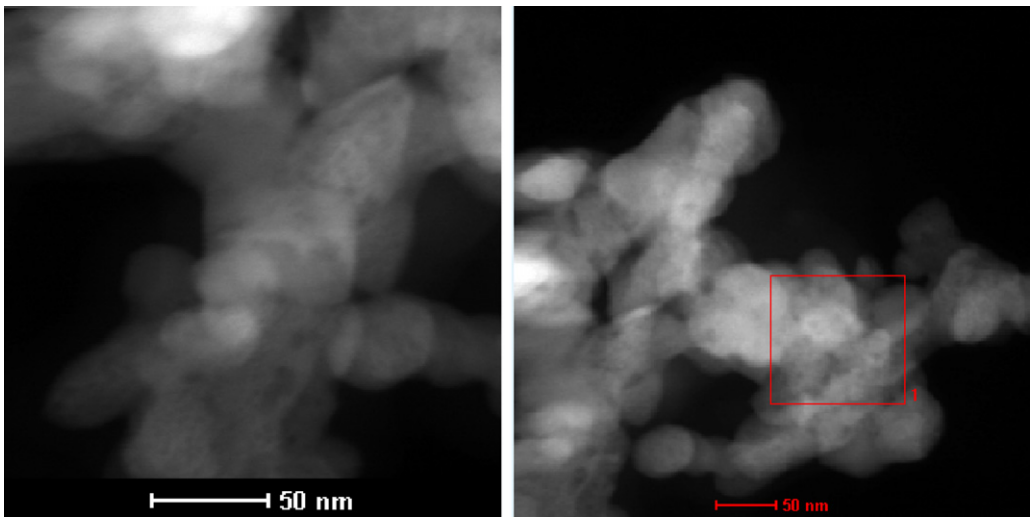

Fig. 6. STEM photograph of 1 wt% Ag/$La_{0.8}Ba_{0.2}MnO_3$.

a lower magnification (150×) of bare support shows the regular structure of cordierite honeycomb and very clear presence of perovskite catalyst on the walls of the support, appeared as dispersed mass. The STEM images of 1 wt% Ag-$La_{0.8}Ba_{0.2}MnO_3$ are shown in Fig. 6. The STEM images show the presence of some small spots of lower brightness and that of different sizes, however, these could not be confirmed through EDX analysis due to their high dispersion. EDX compositional analysis of surface was carried out for both $La_{0.8}Ba_{0.2}MnO_3$ and Ag-$La_{0.8}Ba_{0.2}MnO_3$ and the results are shown in Figs. 7 and 8. EDX pattern of Ag-$La_{0.8}Ba_{0.2}MnO_3$ (Fig. 8(1 and 2)) confirms the presence and excellent dispersion of Ag on the surface of perovskite.

XPS survey spectra acquired in the binding energy range of 0–1150 eV are shown in Fig. 9. Corrections due to charging effects

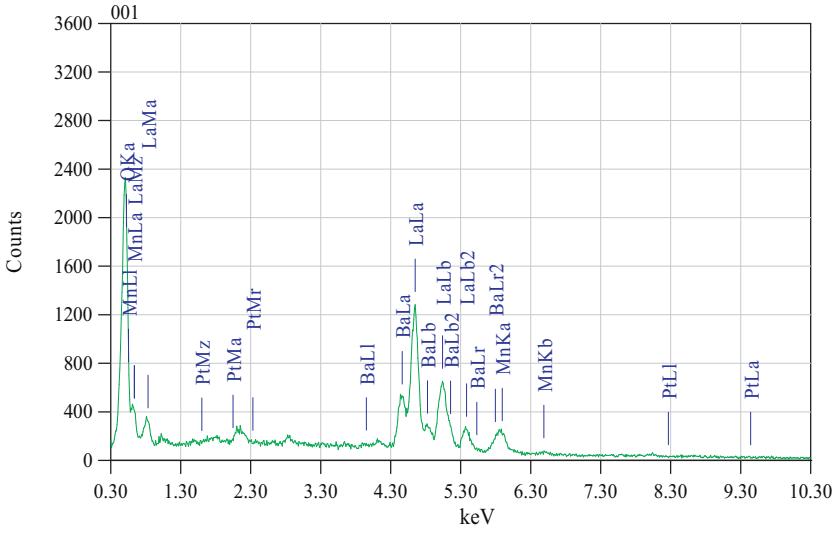

ZAF Method Standardless Quantitative Analysis

Element	(keV)	mass%	Error%	At%
O K	0.525	11.91	0.10	51.71
Mn K	5.894	5.60	0.66	7.08
Ba L	4.464	18.54	0.81	9.38
La L	4.648	62.97	0.94	31.49
Pt M	2.048	0.98	0.59	0.35
Total		100.00		100.00

Fig. 7. EDX pattern for $La_{0.8}Ba_{0.2}MnO_3$.

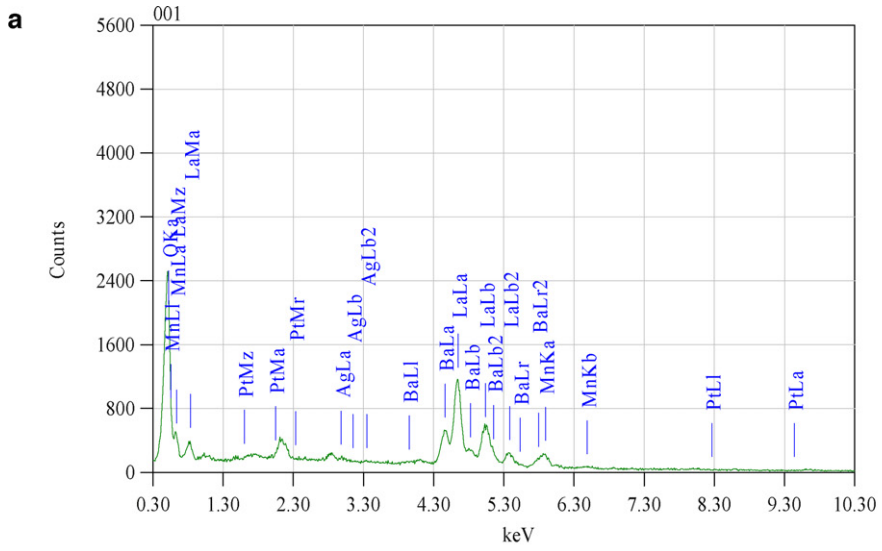

ZAF Method Standardless Quantitative Analysis

Element	(keV)	mass%	Error%	At%
O K	0.525	13.53	0.11	55.41
Mn K	5.894	5.42	0.77	6.46
Ag L	2.983	0.27	0.53	0.17
Ba L	4.464	18.39	0.95	8.77
La L	4.648	60.63	1.09	28.60
Pt M	2.048	1.76	0.69	0.59
Total		100.00		100.00

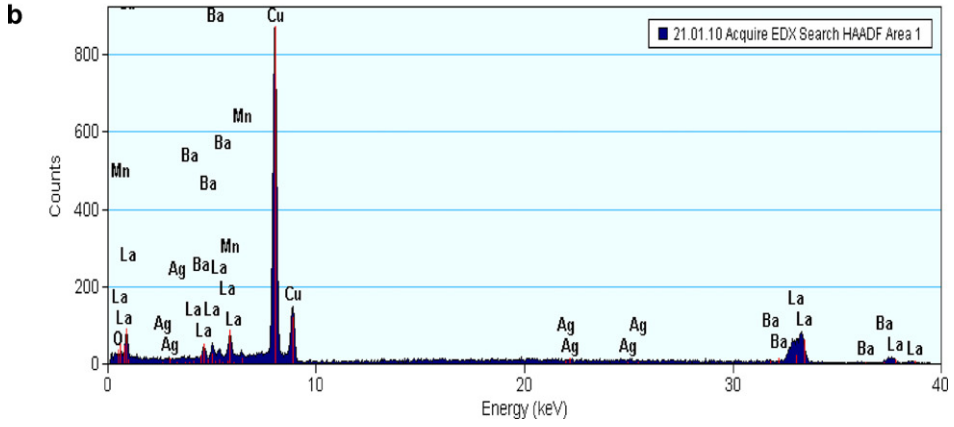

Fig. 8. (1) EDX pattern for 0.05 wt% Ag/$La_{0.8}Ba_{0.2}MnO_3$. (2) EDX (STEM) pattern for 1 wt% Ag/$La_{0.8}Ba_{0.2}MnO_3$.

Table 3
Binding energy (eV) results of surface elements (C 1s at 285 eV) as obtained by XPS analysis.

Catalysts	BE (eV)						ΔE			
	La $3d_{5/2}$	La $3d_{3/2}$	Ba $3d_{5/2}$	Ba $3d_{3/2}$	Mn $2p_{3/2}$	Mn $2p_{1/2}$	O 1s	La	Ba	Mn
$La_{0.8}Ba_{0.2}MnO_3$	838.25	854.95	779.8	795.8	642.9	655.75	529.6	16.7	16	12.85
1 wt% Ag-$La_{0.8}Ba_{0.2}MnO_3$	838.7	855.5	779.8	795.05	643.3	654.85	530.5	16.8	15.25	11.55

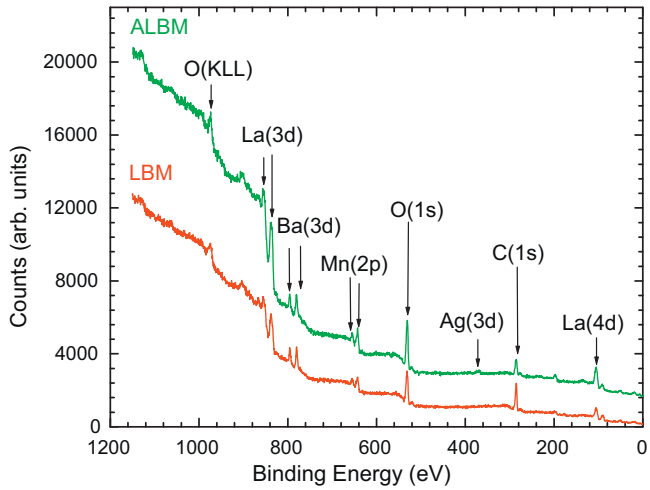

Fig. 9. XPS surveys scan Spectra for $La_{0.8}Ba_{0.2}MnO_3$ (LBM) and 1 wt% Ag/$La_{0.8}Ba_{0.2}MnO_3$ (ALBM).

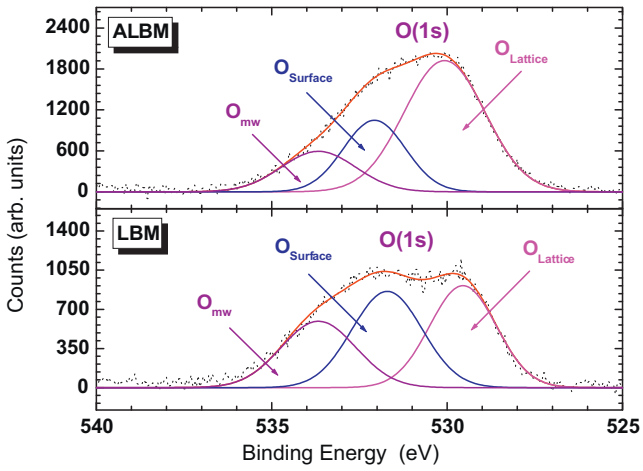

Fig. 11. XPS deconvoluted spectra for O1s core level: $La_{0.8}Ba_{0.2}MnO_3$ (LBM) and 1 wt% Ag/$La_{0.8}Ba_{0.2}MnO_3$ (ALBM).

were taken care of by using C 1s as an internal reference and the Fermi edge of a gold sample. Peak areas were estimated by integrating the appropriate signals after data analysis. During photoemission studies, small specimen charging was observed, which was later calibrated by assigning the C 1s signal at 285 eV for both samples (i.e. $La_{0.8}Ba_{0.2}MnO_3$ and 1 wt% Ag-$La_{0.8}Ba_{0.2}MnO_3$). Survey spectra for sample $La_{0.8}Ba_{0.2}MnO_3$ (Fig. 9) show sharp peaks of La, Ba, Mn, C, and O while 1 wt% Ag-$La_{0.8}Ba_{0.2}MnO_3$ shows the presence of Ag, through a weak signal at 367.5 eV (Fig. 9) [37]. The binding energy values of the observed elements present in Table 3 are in good agreement with standard values.

Our systematic XPS investigations carried out on 1 wt% Ag-$La_{0.8}Ba_{0.2}MnO_3$ compound have revealed that Ag incorporation into the system significantly affect the valence state of Mn. To identify the change in valence state of Mn, core level Mn spectra were analysed using peakfit programme. Peak deconvolution was performed for both the compounds ($La_{0.8}Ba_{0.2}MnO_3$ and 1 wt% Ag-$La_{0.8}Ba_{0.2}MnO_3$), at the same time on Mn($2p_{3/2}$) and Mn($2p_{1/2}$) states, with linear background subtraction and peaks were fitted with Gaussian component, which reveal deconvoluted Mn^{3+} and Mn^{4+} components. Satellite peaks (S_1 and S_2) were also introduced to obtain the best fit. Fig. 10 shows the deconvoluted XPS Mn core-level spectra in the binding energy range 635–665 eV,

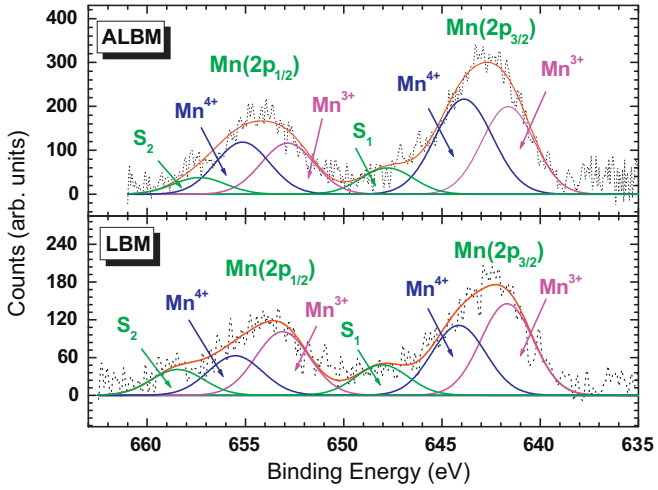

Fig. 10. XPS deconvoluted spectra for Mn2p core level: $La_{0.8}Ba_{0.2}MnO_3$ (LBM) and 1 wt% Ag/$La_{0.8}Ba_{0.2}MnO_3$ (ALBM).

obtained for $La_{0.8}Ba_{0.2}MnO_3$, as those with Ag incorporation. The $La_{0.8}Ba_{0.2}MnO_3$ compound shows the spin–orbit splitting of the Mn 2p level, manifested as Mn$2p_{3/2}$ and Mn$2p_{1/2}$. The difference between these two Mn peaks is 11.55 eV, which indicates the presence of Mn in Mn^{4+} state in perovskite structure. However, deconvoluting the peaks into Gaussian components using appropriate positions and FWHM, shows that Mn exists in both Mn^{3+} (641.7, 653.1 eV) and Mn^{4+} (644.1, 655.5 eV) oxidation states in $La_{0.8}Ba_{0.2}MnO_3$. In addition, characteristic shake-up satellite peaks are observed at 648 and 658 eV, respectively. The results of the XPS studies and consequent deconvolution into Gaussian components showed that Ag incorporation significantly alters the oxidation state of Mn and it changes from Mn^{3+} 48.1% to 41.1% and Mn^{4+} 34.6% to 46.3% as shown in Table 4. This suggests incorporation of Ag in perovskite structure.

To study the effect on surface oxygen defects, deconvolution was performed on O (1s) core level spectra. Fig. 11 shows the deconvoluted spectra of oxygen, which has two peak structure. The peak $O_{lattice}$ is characteristic peak of "O^{2-}" ions of the lattice oxygen and appears at 529.5 eV, while peak $O_{surface}$ appears at 531.7 eV denotes O (1s) surface structure. This surface peak corresponds to the ionization of weakly adsorbed species [33,38] and also the ionization of oxygen ions with particular coordinates, more specifically integrated in the subsurface. This suggests that the existence in the subsurface of oxygen ions that bear lower electron density than the "O^{2-}" ions. In general, these oxide ions can be described as "O^{-}" species [39]. While third peak O_{mw} observed at 533.7 eV is attributed to absorbed molecular water above 532 eV [33,40,41]. When the density of lattice oxygen varies, the area ratio of these three peaks also changes. It is evident from Fig. 11 that Ag incorporation increases $O_{lattice}$ from 36.7% to 58.9%, while $O_{surface}$ and O_{mw} decreases from (shown in Table 4) 36.5% to 24.5% and 26.8% to 16.7%, respectively. Clearly the XPS analysis indicates towards the altered redox states of $La_{0.8}Ba_{0.2}MnO_3$ material after incorporation of Ag, which further suggests the possibility of Ag substitution in perovskite phase.

3.2. Catalytic activity

The catalytic activity results for $LaMnO_3$, $La_{0.8}Ba_{0.2}MnO_3$, various Ag/$La_{0.8}Ba_{0.2}MnO_3$ catalysts and supported catalysts are presented in Figs. 12–15. Pure $LaMnO_3$ perovskite shows considerable activity towards N_2O decomposition at higher temperature but the activity was insignificant at temperature below 400 °C. Presence of NO and O_2 deteriorate the catalytic activity of this catalyst.

Table 4
Quantitative results (%) of Mn and O species as derived from XPS analysis.

Catalysts	Mn $2p_{3/2}$		Mn $2p_{1/2}$		$O_{lattice}$	$O_{surface}$	$O_{surface}$ (adsorbed water molecule)
	Mn^{3+}	Mn^{4+}	Mn^{3+}	Mn^{4+}			
$La_{0.8}Ba_{0.2}MnO_3$	28.1	22.1	20	12.5	36.7	36.5	26.8
1 wt% Ag-$La_{0.8}Ba_{0.2}MnO_3$	25.7	30.5	15.4	15.8	58.9	24.5	16.7

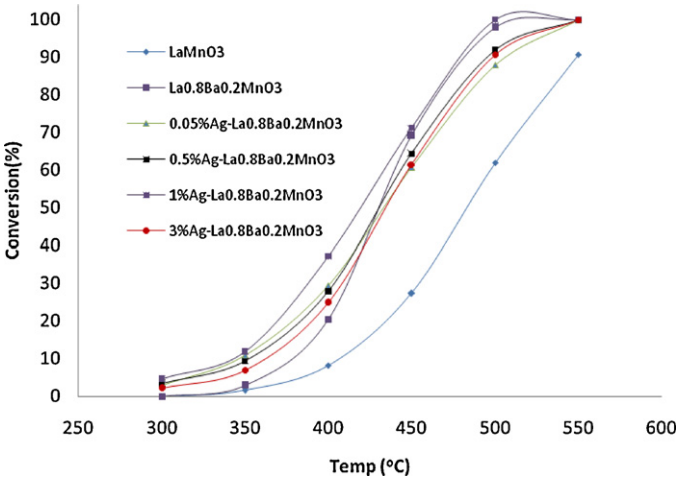

Fig. 12. N_2O decomposition as a function of temperature for $LaMnO_3$, $La_{0.8}Ba_{0.2}MnO_3$ and various $Ag/La_{0.8}Ba_{0.2}MnO_3$ catalysts.

Significant increase in activity was achieved after the incorporation of Ba in perovskite structure. At 500 °C, the catalytic activity of $LaMnO_3$ was about 62%, which was observed to be almost 100% in case of Ba incorporated perovskite catalyst. In this way, Ba substitution results in substantial improvement in N_2O decomposition activity of the present catalyst. This is mainly due to the altered redox properties of lanthanum manganate perovskite, as also substantiated by XPS and TPR results. It was planned to study the effect of Ag incorporation, possibly to further improve the catalytic activity, as the silver is often reported to promote NOx catalytic activity. Z. Liu [33] observed the promotional effect of Ag on $La_{0.8}Ce_{0.2}CoO_3$ catalyst for direct decomposition and reduction of NO. From this observation, we also inferred that Ag could be the promoter to improve the catalytic activity of $La_{0.8}Ba_{0.2}MnO_3$ for N_2O decomposition in presence of catalytic inhibitors such as oxygen and water vapour.

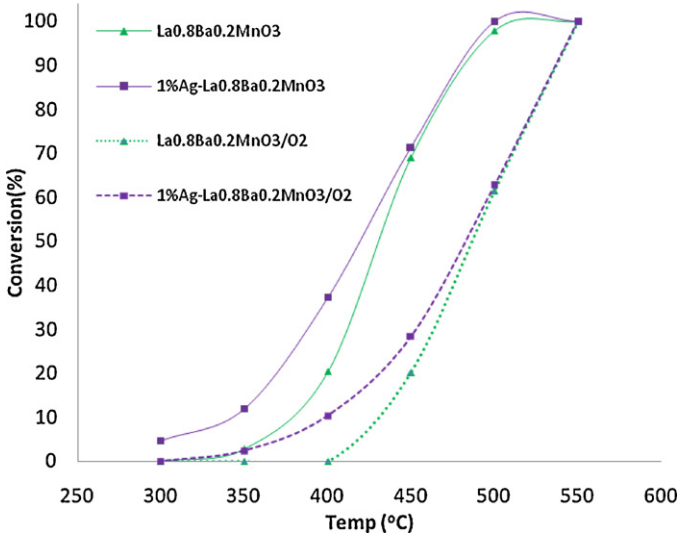

Fig. 13. N_2O decomposition as a function of temperature for $La_{0.8}Ba_{0.2}MnO_3$ and 1 wt% $Ag/La_{0.8}Ba_{0.2}MnO_3$ in presence 5 vol% $.O_2$.

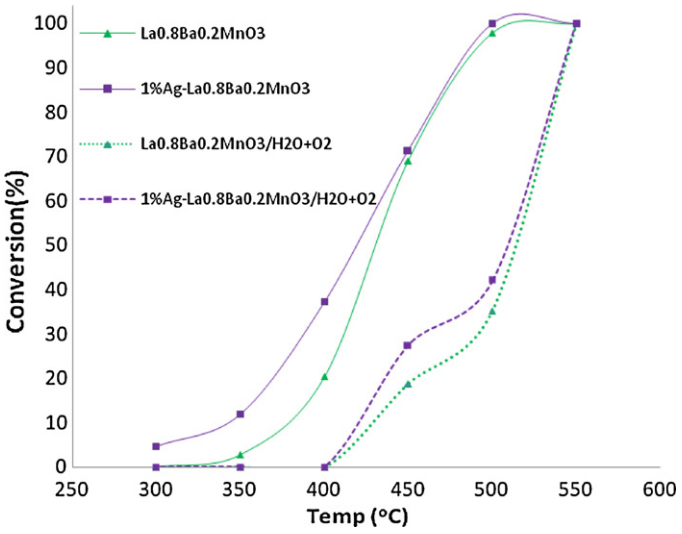

Fig. 14. N_2O decomposition as a function of temperature for $La_{0.8}Ba_{0.2}MnO_3$ and 1 wt% $Ag/La_{0.8}Ba_{0.2}MnO_3$ in the presence of 3 vol% H_2O and 5 vol% O_2.

3.2.1. *Effect of Ag loading on N_2O decomposition activity*

In order to investigate the details of promotional effect of Ag on $La_{0.8}Ba_{0.2}MnO_3$ for N_2O decomposition, Ag doped $La_{0.8}Ba_{0.2}MnO_3$ compositions were prepared with different Ag content. These catalysts were evaluated for their catalytic activity and effect of other gases, and the results are given in Fig. 12. The effect of Ag promotion was more significant below 450 °C for $La_{0.8}Ba_{0.2}MnO_3$ catalyst, which suggests that the low temperature activity is due to the presence and selectivity of Ag. Liu et al. also reported that Ag

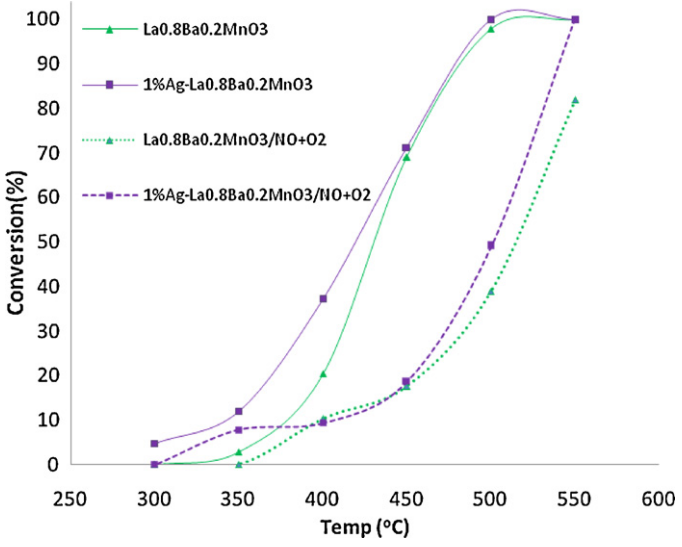

Fig. 15. N_2O decomposition as a function of temperature for $La_{0.8}Ba_{0.2}MnO_3$ and 1 wt% $Ag/La_{0.8}Ba_{0.2}MnO_3$ in presence 0.02 vol% NO and 5 vol% O_2.

promotion increases the catalytic activity of $La_{0.6}Ce_{0.4}CoO_3$ below 500 °C for NO reduction [33]. The activity of $La_{0.8}Ba_{0.2}MnO_3$ catalyst was observed to be maximum at 1 wt% Ag loading. This catalyst shows T_{50} at 418 °C while 100% N_2O decomposition was observed at 495 °C. Hence, 1 wt% loading of Ag for this perovskite is considered as optimum and further studies were carried out using this composition only.

3.2.2. Effect of O_2 on N_2O decomposition activity

Inhibition of catalytic activity by oxygen remains one of the important challenges towards catalytic decomposition of N_2O. The effect of 5 vol% oxygen on N_2O decomposition for $La_{0.8}Ba_{0.2}MnO_3$ and 1 wt% Ag-$La_{0.8}Ba_{0.2}MnO_3$ catalysts were investigated and the results are shown in Fig. 13. At high temperature, no significant effect was observed for both bare and promoted catalysts, however, un-promoted catalyst shows significant lowering of activity below 550 °C in the presence of oxygen.

3.2.3. Effect of O_2 and water vapour on N_2O decomposition activity

In order to investigate the effect of water vapour on N_2O decomposition activity of bare and promoted catalysts, approximately 3 vol% water was introduced in the feed along with 5 vol% oxygen. As inferred from Fig. 14, the activity remains almost unchanged for both at high temperature for $La_{0.8}Ba_{0.2}MnO_3$ and 1 wt% Ag-$La_{0.8}Ba_{0.2}MnO_3$ catalysts, however, the Ag promoted catalyst shows better activity in the temperature window of 400–500 °C.

3.2.4. Effect of NO and O_2 on N_2O decomposition activity

The catalytic activity of $La_{0.8}Ba_{0.2}MnO_3$ and 1 wt% Ag-$La_{0.8}Ba_{0.2}MnO_3$ for N_2O decomposition was also evaluated in presence of 5 vol% O_2 and 0.02 vol% NO. As shown in Fig. 15, both the catalysts show decrease in activity, however, this effect was more pronounced in case of $La_{0.8}Ba_{0.2}MnO_3$. In case of 1 wt% Ag-$La_{0.8}Ba_{0.2}MnO_3$ this effect was significant below 450 °C only. From these results, we observed that the promotional effect of NO on catalytic N_2O decomposition is not significant for present catalysts, and that the activity mainly depends on the altered redox properties of perovskite compositions.

Fig. 16 shows reaction rate for N_2O decomposition in presence of oxygen and NO for the $La_{0.8}Ba_{0.2}MnO_3$ and 1 wt%Ag-$La_{0.8}Ba_{0.2}MnO_3$ catalysts. Reaction rate was calculated as millimoles of N_2O converted per g of catalyst per unit time. Maximum

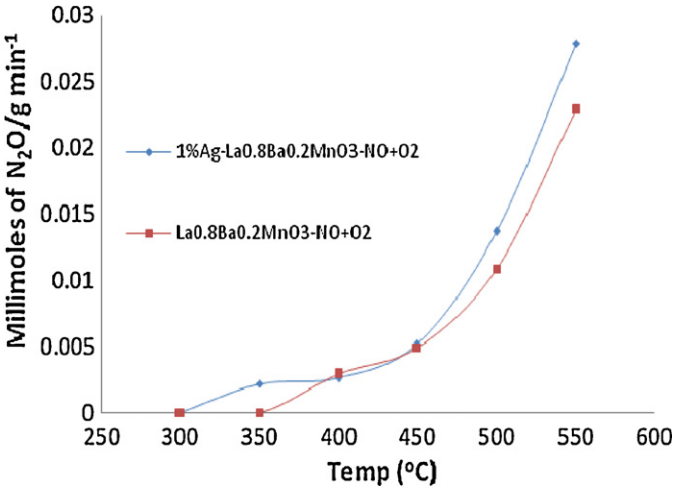

Fig. 16. N_2O decomposition reaction rate as a function of temperature for $La_{0.8}Ba_{0.2}MnO_3$ and 1 wt% Ag/$La_{0.8}Ba_{0.2}MnO_3$ in the presence of 0.02 vol% NO and 5 vol% O_2.

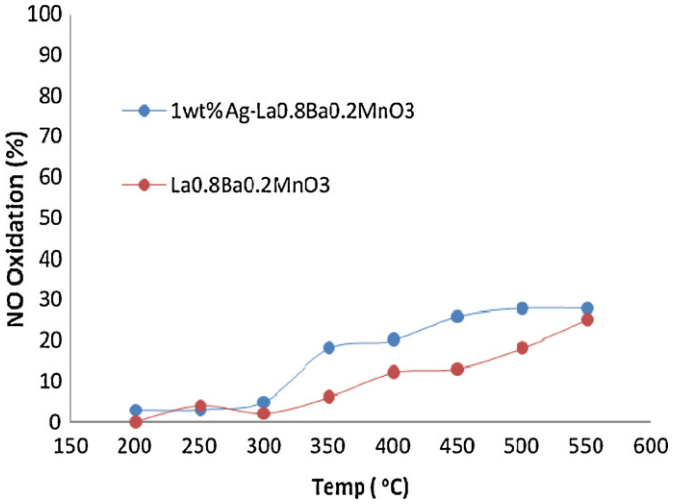

Fig. 17. NO oxidation as a function of temperature for $La_{0.8}Ba_{0.2}MnO_3$ and 1 wt% Ag/$La_{0.8}Ba_{0.2}MnO_3$.

0.028 mmol of N_2O were converted per g of catalyst per min, when 1 wt% Ag-$La_{0.8}Ba_{0.2}MnO_3$ shows the 100% N_2O conversion at 550 °C. $La_{0.8}Ba_{0.2}MnO_3$ converts a maximum of 0.023 mmol of N_2O at about 550 °C. Both the catalysts show overall excellent catalytic activity for the N_2O decomposition reaction and the activity observed is considerably improved as compared to unsubstituted $LaMnO_3$ catalyst.

In nitric acid industry tail gas, NO is often co-existing with N_2O, depending on the process control and application of after-exhaust NO control technology like SCR. The zeolite based N_2O decomposition catalysts are reported to show NO oxidation, which in turn also increase the N_2O decomposition activity. In order to investigate this effect, the NO conversion was also followed while studying the effect of NO on N_2O decomposition activity. As indicated in Fig. 17, both the catalysts show only moderate activity for NO conversion, which primarily appears to be due to oxidation at lower temperature and decomposition at higher temperatures as, inferred from the total NO_x data (mass balance).

3.2.5. Catalytic activity of supported catalysts

Ceramic honeycomb supported catalytic materials were also evaluated for their N_2O decomposition activity in the presence of NO and O_2. Fig. 18 presents the catalytic evaluation results obtained with the perovskite catalyst coated ceramic honeycomb supports, prepared by in situ synthesis technique. As indicated in Fig. 18, the activity of supported $La_{0.8}Ba_{0.2}MnO_3$ and Ag/$La_{0.8}Ba_{0.2}MnO_3$ at 550 °C shows 55 and 100% N_2O conversion, respectively. The catalytic performance of supported catalysts is almost similar to that obtained for powder samples. The catalytic activity of supported catalyst was slightly better than the powder catalyst at lower temperature (≤350 °C), which could be due to better mass transfer.

3.2.6. Catalyst stability

For industrial applications, catalyst stability is an important criterion for a potential catalyst. Stability of the 1 wt% Ag-$La_{0.8}Ba_{0.2}MnO_3$ catalyst for N_2O decomposition was examined at 550 °C and the results are shown in Fig. 19. The Ag promoted present perovskite catalyst shows no adverse effect in presence of 200 ppm NO and 5% O_2 in the feed. At 550 °C, the catalyst shows ≥90% N_2O conversion even after 30 h exposure to simulated feed. It is found that the structure of 1 wt% Ag-$La_{0.8}Ba_{0.2}MnO_3$ remains intact after 30 h of reaction exposure, which is confirmed by XRD studies of used sample as shown in Fig. 20.

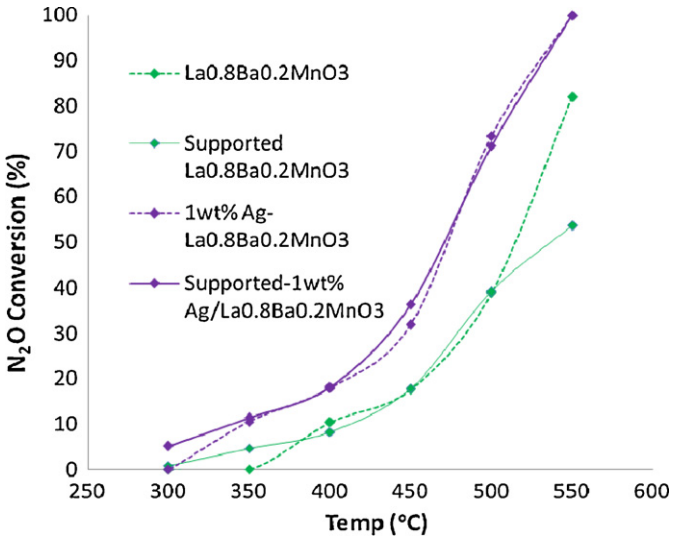

Fig. 18. N_2O decomposition as a function of temperature for supported-$La_{0.8}Ba_{0.2}MnO_3$ and supported-1 wt% $Ag/La_{0.8}Ba_{0.2}MnO_3$ in the presence of 0.02 vol% NO and 5 vol% O_2.

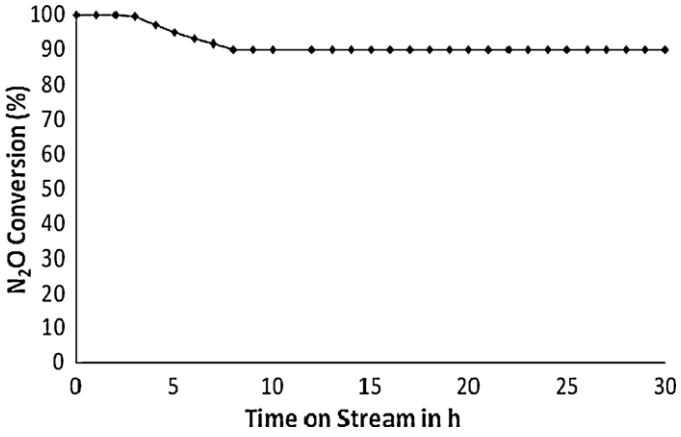

Fig. 19. 'Time on stream' behavior for 1 wt% $Ag/La_{0.8}Ba_{0.2}MnO_3$ catalyst for N_2O decomposition in presence 0.02 vol% NO and 5 vol% O_2.

3.2.7. *Mechanistic aspects*

There are few reaction mechanisms proposed for the catalytic decomposition of N_2O, which mainly depends on catalyst composition as well as promoter elements used. The N_2O decomposition over oxide catalysts involves a redox mechanism as reported by different researchers [42–49]. It is generally accepted that surface vacant sites are responsible for nitrous oxide decomposition. In this redox mechanism, N_2O acts as an oxidizing agent and oxygen is desorbed in the reducing step. In case of perovskite, the nitrous oxide catalytic decomposition proceeds mainly in three steps. The step (1) would be the adsorption of N_2O molecule on the surface vacant site, (2) desorption of this surface adsorbed oxygen by combining with another oxygen atom and by forming O_2 to gas phase, (3) or means of directly reacting with N_2O molecule. Probably steps (1) and (3) are irreversible, while (2) is reversible.

$$M\text{–}V_O\text{–}M + N_2O \rightarrow M\text{–}O\text{–}M + N_2 \quad \text{(step1)}$$

$$2M\text{–}O\text{–}M \leftrightarrows 2M\text{–}V_O\text{–}M + O_2 \quad \text{(step2)}$$

$$N_2O + M\text{–}O\text{–}M \rightarrow M\text{–}V_O\text{–}M + O_2 + N_2 \quad \text{(step3)}$$

where V_O is the surface vacant site.

For $La_{0.8}Ba_{0.2}MnO_3$ the N_2O catalytic decomposition activity is higher than that of $LaMnO_3$. This is due to oxygen non-stoichiometry in $La_{0.8}Ba_{0.2}MnO_3$ through partial substitution of bivalent Ba at 'A' site. This substitution alters the oxidation state of 'B' site cation. In $LaMnO_3$ 'B', cation is in the oxidation state of +3 but in partially substituted $La_{0.8}Ba_{0.2}MnO_3$, 'B' cation adjusts to mixed oxidation state of +3 and +4, depending on the degree of substitution. In case of silver promoted $La_{0.8}Ba_{0.2}MnO_3$ the N_2O decomposition activity is further improved, which could be due to the increase of Mn^{4+}/Mn^{3+} ratio. Some of Ag ions doped on to the surface of $La_{0.8}Ba_{0.2}MnO_3$ may partially occupy the La sites due to their similar ionic radii. Because of this Ag incorporation in lattice structure, the amount of Mn^{4+} is increased in Ag promoted perovskite. In this way, the altered redox properties of perovskite appears to be the most likely cause for improved catalytic activity of Ag promoted Ba substitute lanthanum manganate catalyst. The XPS study findings support this hypothesis through observed improved Mn^{4+}/Mn^{3+} ratio in barium substituted as well as in silver promoted $LaMnO_3$ compositions. To further substantiate the altered redox properties of present catalysts, oxygen-TPD and hydrogen-TPR studies have been performed.

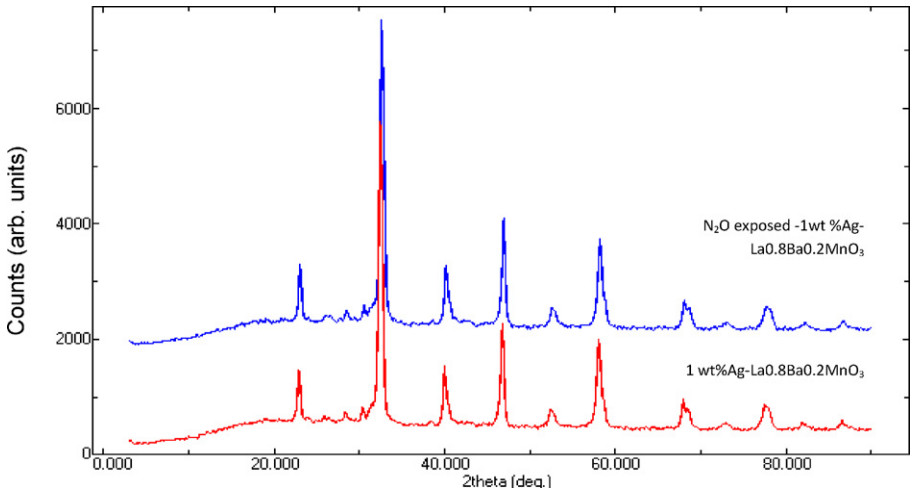

Fig. 20. XRD pattern for 1 wt% $Ag/La_{0.8}Ba_{0.2}MnO_3$ and N_2O exposed 1 wt% $Ag/La_{0.8}Ba_{0.2}MnO_3$.

3.2.8. Oxygen temperature programmed desorption studies

Oxygen-temperature programmed desorption (O_2-TPD) was carried out to study the oxygen non-stoichiometry of substituted perovskite, and to understand its role in N_2O decomposition. Generally, oxygen defects are formed when a perovskite is heated at high temperature. Two different types of oxygen are known for perovskite i.e. α-oxygen (suprafacial oxygen) desorbed at relatively lower temperature and β oxygen (intrafacial oxygen), which is desorbed at high temperature [28]. The α and β oxygen usually belong to surface and bulk respectively. When divalent Ba is substituted in trivalent A site of $LaMnO_3$ a charge compensation is needed to achieve the electroneutrality. This can either attained by oxygen defects or the shift of the B metal ion towards higher oxidation states (Mn^{3+} and Mn^{4+}).

As indicated in Fig. 21, the strong high temperature peak corresponding to lattice oxygen desorption was shifted to higher temperature with Ba partial substitution, while this peak became further stronger with Ag incorporation. The high temperature oxygen desorption of $LaMnO_3$ is usually referred as release of oxygen-excess non-stoichiometry. This is usually due to the formation of Mn^{4+} in $LaMnO_3$ to reduce the Jahn–Teller distortion, although the charge balance suggests that Mn should be in 3+ oxidation state. In $La_{0.8}Ba_{0.2}MnO_3$ the Mn^{4+} state is more stable due to the presence of Ba^{2+} ions in lattice (charge compensation) [28]. In case of 1 wt% Ag-$La_{0.8}Ba_{0.2}MnO_3$ the Mn^{4+} state is even more stable than $La_{0.8}Ba_{0.2}MnO_3$ due to the presence Ba^{2+} as well as Ag^{+} ions at 'A' site of perovskite structure. Accordingly, the lattice oxygen desorption peak is shifted to higher temperature in these compounds. We can infer from this observation, that the Ag incorporation increases the Mn^{4+}/Mn^{3+} ratio of $La_{0.8}Ba_{0.2}MnO_3$ catalyst as also observed in XPS analysis.

3.2.9. Temperature programmed reduction (TPR) studies

The H_2-TPR studies of all the three catalysts have been carried out to examine the reducibility of different catalyst compositions. The H_2-TPR profile of these catalysts $LaMnO_3$, $La_{0.8}Ba_{0.2}MnO_3$ and 1 wt% Ag-$La_{0.8}Ba_{0.2}MnO_3$ are shown in Fig. 22. Two major reduction peaks were observed; first low temperature peak in the range of 100–530 °C, which should belong to the reduction of Mn^{4+} to Mn^{3+} and the second high temperature hydrogen consumption peak in the range of 580–800 °C, which could be due to the reduction of Mn^{3+} to Mn^{2+}. $LaMnO_3$ shows a reduction peak for Mn^{4+} to Mn^{3+} due to over stoichiometry as already mentioned in O_2-TPD studies [28]. The Mn^{4+} reduction peak intensity increased with Ba substitution, indicating the higher content of Mn^{4+}, while this peak became further intense and shifted towards lower temperature for

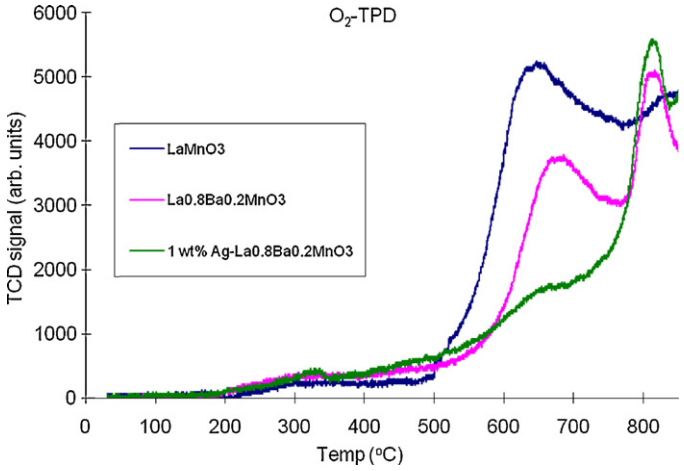

Fig. 21. O_2-TPD profile for $LaMnO_3$, $La_{0.8}Ba_{0.2}MnO_3$ and 1 wt% Ag/$La_{0.8}Ba_{0.2}MnO_3$.

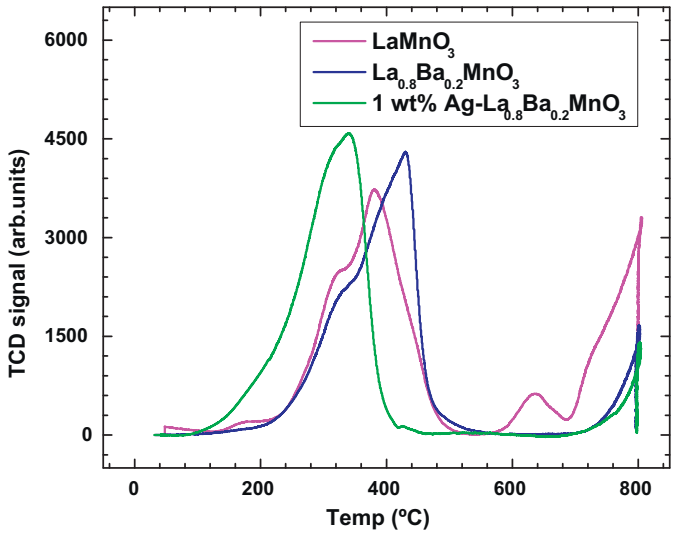

Fig. 22. H_2-TPR profile for $LaMnO_3$, $La_{0.8}Ba_{0.2}MnO_3$ and 1 wt% Ag/$La_{0.8}Ba_{0.2}MnO_3$.

Ag promoted catalyst. Overall improved reduction of Mn^{4+} to Mn^{3+} was observed in case of silver promoted catalyst with higher peak intensity, inferring the altered redox properties for this catalyst. The intensity for second reduction peak of Mn^{3+} to Mn^{2+} decreased with Ba substitution and further decreased by Ag addition. These TPR profiles therefore further substantiate the altered redox properties of perovskite by means of Ba and Ag incorporation, and can explain improved catalytic activity of Ba and Ag promoted catalysts, as also corroborated by XPS and TPD findings. Insignificant effect of NO on N_2O decomposition also infers the different mechanisms operating in present perovskite type catalysts as compared to those zeolite based.

4. Conclusion

$LaMnO_3$ type non-noble metal based perovskite catalysts with Ba substitution and Ag promotion were systematically studied for their catalytic activity towards N_2O decomposition reaction in presence of oxygen, NO and water vapour. These low-cost catalysts have been synthesized by co-precipitation, followed by impregnation method, and studied for their N_2O decomposition activity under different conditions. The catalysts have also been deposited on ceramic honeycomb support, by following the same methods of preparation. Both Ba substitution as well as Ag incorporation show promotional effect on N_2O decomposition activity of $LaMnO_3$ type catalyst. 1 wt%Ag promoted $La_{0.8}Ba_{0.2}MnO_3$ shows 100% N_2O conversion in presence of oxygen and NO at 550 °C with a reaction rate of 0.028 mmol per g of catalyst per min.

The catalyst characterization studies suggest that the improved catalytic activity of Ba as well as Ag promoted catalysts are mainly because of the altered redox properties of $LaMnO_3$. This is primarily the result of the altered Mn^{4+}/Mn^{3+} ratio in these promoted catalysts, because of charge compensation effect. There was an insignificant effect of NO promotion observed, which further suggest the redox mechanism of N_2O decomposition. X-ray photoelectron spectroscopy, O_2-TPD, and H_2-TPR studies of these catalysts also infer the altered redox properties of Ba as well as Ag promoted compositions. This lead us to believe that both Ba and Ag are primarily present in the perovskite structure. The present N_2O decomposition study therefore, contribute towards better understanding of this reaction on perovskite type catalysts, which can be useful for design of catalysts with further improved activity. The

time stream stability study also indicates potential of such low cost catalysts for catalytic N_2O decomposition.

Acknowledgements

This work was carried out under the CSIR Supra-Institutional project No. SIP-16 (3.1) as well as, under the research cooperation between NEERI, India and Kyushu University, Japan under the Global COE Programme of Kyushu University. Some characterization studies were carried out at VNIT and JNARDDC, Nagpur, India.

References

[1] P.L. Crutzen, J. Geophys. Res. 76 (1971) 7311–7327.
[2] J.C. Kramlich, W.P. Linak, Prog. Energy Combust. Sci. 20 (1994) 149–202.
[3] M.A. Wojtowicz, J.R. Pels, J.A. Moulijn, Fuel. Process. Technol. 34 (1993) 1–71.
[4] H. Rodhe, Science 248 (1990) 1217–1219.
[5] A.R. van Amstel, R.J. Steward, Fert. Res. 37 (1994) 213–225.
[6] D.J. Jacob, Introduction to Atmosphere Chemistry, Princeton, New Jersey, 1999.
[7] J.H. Seinfeld, S.N. Pandis, Atmospheric Chemistry and Physics, Wiley Interscience, New York, 1998.
[8] Fourth Assessment Report of the IPCC, Changes in Atmospheric Constituents and in Radiative Forcing (chapter 2), 2007.
[9] Inventory of Greenhouse Gas Emissions and Sinks (1990–2007), U.S. EPA, Washington, 2009.
[10] J.S Choe, P.J Cook, F.P Petrocelli, Presented at ANSPG Conference, Destin, FL, USA, 6 October, 1993, pp. 1–13.
[11] R.A. Reimer, C.S. Slaten, M. Seapan, M.W. Lower, P.E. Tomlinson, Environ. Prog. 13 (1994) 134–137.
[12] G.G.d. Soete, Rev. Inst. Franc. Petr. 48 (1993) 413–451.
[13] J.P. Ramirez, F. Kapteijn, K. Schoffel, J.A. Moulijn, Appl. Catal. B: Environ. 44 (2003) 117–151.
[14] F. Kapteijn, J.R. Mirasol, J.A. Moulijn, Appl. Catal. B: Environ. 9 (1996) 25–64.
[15] P.S.S. Reddy, N. Pasha, M.G.V.C. Rao, N. Lingaiah, I. Suryanarayana, P.S.S. Prasad, Catal. Commun. 8 (2007) 1406–1410.
[16] V.K. Tzitzios, V. Georgakilas, Chemosphere 59 (2005) 887–891.
[17] R. Burch, S.T. Daniells, J.P. Breen, P. Hu, J. Catal. 224 (2004) 252–260.
[18] A. Satsuma, H. Maeshima, K. Watanabe, K. Suzuki, T. Hattori, Catal. Today 63 (2000) 347–353.
[19] F.J.P. Alonso, I.M. Cabrera, M.L. Granados, F. Kapteijn, J.L.G. Fierro, J. Catal. 239 (2006) 340–346.
[20] P. Granger, P. Esteves, S. Kieger, L. Navascues, G. Leclercq, Appl. Catal. B: Environ. 62 (2006) 236–243.
[21] G. Centi, U.S. Perathoner, F. Vazzana, M. Marella, M. Tomaselli, M. Mantegazza, Adv. Environ. Res. 4 (2000) 325–338.
[22] U. Chellam, Z.P. Xu, H.C. Zeng, Chem. Mater. 12 (2000) 650–658.
[23] J. Pieterse, S. Booneveld, R. Bink, Appl. Catal. B: Environ. 51 (2004) 215–228.
[24] J.P. Ramirez, F. Kapteijn, G. Mul, J.A. Moulijn, Chem. Commun. 8 (2001) 693–694.
[25] E.V. Kondratenko, V.A. Kondratenko, M. Santiago, J.P. Ramírez, J. Catal. 256 (2008) 248–258.
[26] R.W. van den Brink, S. Booneveld, J.R. Pels, D.F. Bakker, M.J.F.M. Verhaak, Appl. Catal. B: Environ. 5 (1995) 32 (2001) 73–81.
[27] C.S. Swamy, J. Cristopher, Cat. Rev. Sci. Eng. 34 (1992) 409–425.
[28] N. Yamazoe, Y. teraoka, Catal. Today 8 (1990) 175–199.
[29] L.G. Tejuca, J.L. Fierro, J.M.D. Tascon, Adv. Catal. 36 (1989) 237–328.
[30] N. Russo, D. Mescia, D. Fino, G. Saracco, V. Specchia, Ind. Eng. Chem. Res. 46 (2007) 4226–4231.
[31] S. Alini, F. Basile, S. Blasioli, C. Rinaldi, A. Vaccari, Appl. Catal. B: Environ. 70 (2007) 323–329.
[32] F.C. Buciuman, E. Joubert, J.C. Menezo, J. Barbier, Appl. Catal. B: Environ. 35 (2001) 149–156.
[33] Z. Liu, J. Hao, L. Fu, T. Zhu, Appl. Catal. B: Environ. 44 (2003) 355–370.
[34] J. Zhu, A. Thomas, Appl. Catal. B: Environ. 92 (2009) 225–233.
[35] J.P. Dacquin, C. Dujardin, P. Granger, Catal. Today 137 (2008) 390–396.
[36] N.K. Labhsetwar, A. Watanabe, R.B. Biniwale, R. Kumar, T. Mitsuhashi, Appl. Catal. B: Environ. 867 (2001) 1–9.
[37] E. Gulari, C. Guldur, S. Srivannavit, S. Osuwan, Appl. Catal. A 182 (1999) 147.
[38] W. Cao, O.K. Tan, W. Zhu, J.S. Pan, J. Bin, IEEE Sens. J. 3 (2003) 421–434.
[39] J.C. Dupin, D. Gonbeau, P. Vinatier, A. Levasseur, Phys. Chem. Chem. Phys. 2 (2000) 1319–1324.
[40] A. Machocki, T. Ioannides, B. Stasinska, W. Gac, G. Avgouropoulos, D. Delimaris, W. Grzegorczyk, S. Pasieczna, J. Catal. 227 (2004) 282–296.
[41] S. Ponce, M.A. Pena, J.L.G. Fierro, Appl. Catal. B Environ. 24 (2000) 193–205.
[42] D. Nakashima, Y. Ichihashi, S. Nishiyama, S. Tsuruya, J. Mol. Catal. A: Chem. 259 (2006) 108–115.
[43] Y. Li, D. Nakashima, Y. Ichihashi, S. Nishiyama, S. Tsuruya, Ind. Eng. Chem. Res. 43 (2004) 6021–6026.
[44] K. Asano, C. Ohnishi, S. Iwamoto, Y. Shioya, M. Inoue, Appl. Catal. B: Environ. 78 (2008) 242–249.
[45] L. Xue, C. Zhang, H. He, Y. Teraoka, Catal. Today 126 (2007) 449–455.
[46] N. Russo, D. Fino, G. Saracco, V. Specchia, Catal. Today 119 (2007) 228–232.
[47] F. Pinna, M. Scarpa, G. Strukul, E. Guglielminotti, F. Boccuzzi, M. Manzoli, J. Catal. 192 (2000) 158–162.
[48] P.E. Fanning, M.A. Vannice, J. Catal. 207 (2002) 166–182.
[49] T. Nobukawa, M. Yoshida, K. Okumura, K. Tomishige, K. Kunimori, J. Catal. 229 (2005) 374–388.